Bull Volcanol (1994) 56:193–206

Bulletin of
Volcanology

Quantifying the effect of rheology on lava-flow margins using fractal geometry

B. C. Bruno[1], **G. J. Taylor**[1], **S. K. Rowland**[1], **S. M. Baloga**[2]*

[1] Hawaii Institute of Geophysics and Planetology, University of Hawaii at Manoa, 2525 Correa Road, Honolulu, Hawaii 96822, USA
[2] Jet Propulsion Laboratory, NASA, California Institute of Technology, 4800 Oak Grove Drive, Pasadena, California 91109, USA

Received: June 6, 1993/Accepted: March 18, 1994

Abstract. This study aims at quantifying the effect of rheology on plan-view shapes of lava flows using fractal geometry. Plan-view shapes of lava flows are important because they reflect the processes governing flow emplacement and may provide insight into lava-flow rheology and dynamics. In our earlier investigation (Bruno et al. 1992), we reported that flow margins of basalts are fractal, having a characteristic shape regardless of scale. We also found we could use fractal dimension (D, a parameter which quantifies flow-margin convolution) to distinguish between the two endmember types of basalts: a'a (D: 1.05–1.09) and pahoehoe (D: 1.13–1.23). In this work, we confirm those earlier results for basalts based on a larger database and over a wider range of scale (0.125 m–2.4 km). Additionally, we analyze ten silicic flows (SiO_2: 52–74%) over a similar scale range (10 m–4.5 km). We note that silicic flows tend to exhibit scale-dependent, or non-fractal, behavior. We attribute this breakdown of fractal behavior at increased silica contents to the suppression of small-scale features in the flow margin, due to the higher viscosities and yield strengths of silicic flows. These results suggest we can use the fractal properties of flow margins as a remote-sensing tool to distinguish flow types. Our evaluation of the nonlinear aspects of flow dynamics indicates a tendency toward fractal behavior for basaltic lavas whose flow is controlled by internal fluid dynamic processes. For silicic flows, or basaltic flows whose flow is controlled by steep slopes, our evaluation indicates non-fractal behavior, consistent with our observations.

Key words: fractals – lava – rheology – remote sensing

* *Present address:* Proxemy Research Inc., 20528 Farcroft Lane, Laytonsville, Maryland 20882, USA

Correspondence to: B. C. Bruno

Introduction

Plan-view shapes of lava flows reflect the processes governing flow emplacement; they are frozen snapshots of the final moments of flow. As such, they provide insight into the final stages of lava-flow dynamics and rheological state. Plan-view shapes and other morphological characteristics have been studied extensively and important quantitative parameters have been developed to extract rheological properties and eruption and emplacement processes of lava flows. Useful parameters include flow length and width as indicators of eruption rate and duration (Walker 1973; Hulme and Fielder 1977); widths and thicknesses of flows to estimate yield strengths (Hulme 1974); widths of distal lobes to deduce rheological properties and SiO_2 content (Wadge and Lopes 1991); channel depth and width and surface speed to estimate viscosity (Shaw et al. 1968); total area and volume to estimate maximum flow rates and minimum emplacement times (Shaw and Swanson 1970); flow length and width coupled with levee and channel width to yield effusion rate (Crisp and Baloga 1990); average thickness and the ratio of maximum width to maximum length to calculate eruption duration (Lopes and Kilburn 1990); and ridge heights and spacings to estimate viscosity of flow interiors (Fink and Fletcher 1978; Fink 1980). Use of these measurements has led to improved insight into lava-flow dynamics and planetary volcanism, but many questions about their quantitative use remain.

We have been using a new approach to quantitatively characterize lava-flow morphology: the fractal properties of flow margins. In our preliminary report (Bruno et al. 1992), we showed that the perimeters of basaltic flows are fractal, and have characteristic fractal dimensions. Fractals are objects (real or mathematical) that look the same at all scales (Mandelbrot 1967, 1983). Many geologic features exhibit such 'self-similar' behavior (e.g. rocky coastlines, topography, river networks). A qualitative example of self-similar behavior of a lava-flow margin appears in Fig. 1. We believe that measurement of fractal properties of lava flows

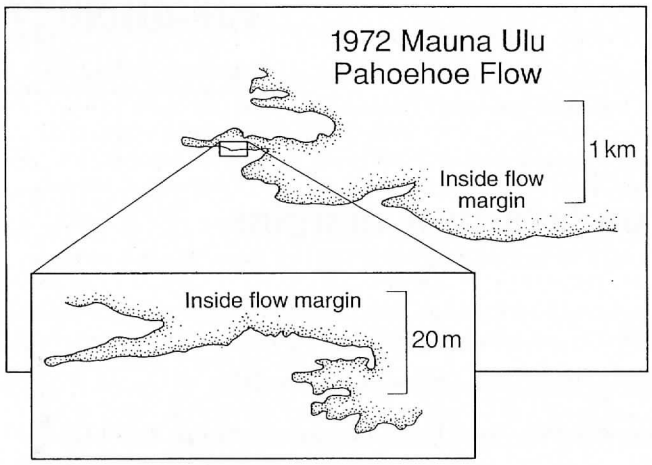

Fig. 1. Margin of a typical pahoehoe flow from the 1972 eruption of Mauna Ulu, Kilauea volcano with small section enlarged to show self-similarity. The similar shapes of the entire flow margin and the enlarged section at different scales suggests fractal behavior

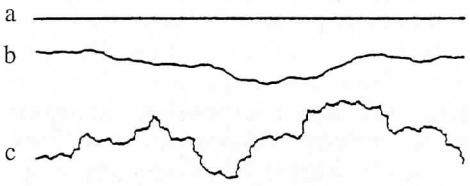

Fig. 2 Fractal dimensions (D) of selected curves: **a** $D=1.00$; **b** $D=1.01$; **c** $D=1.10$. The complex curves (b, c) are longer and are more plane-filling than (a) and thus have $D>1$. Since these curves are contained in a plane ($D=2$), they have D between 1 and 2 (following Garcia 1991)

will shed light on flow dynamics, eruption rates, and rheology, and will prove to be a useful method for quantifying the morphology of lava flows in inaccessible areas of the Earth as well as on other planets by means of remote sensing.

The key parameter we derive is fractal dimension. Fractal dimension (D) is based on a similar concept as topological dimension (D_T). For example, a line can be contained in a plane; thus a line ($D_T=1$) has a lower topological dimension than a plane ($D_T=2$). Similarly, a plane can be contained in a volume; thus a volume has a greater topological dimension ($D_T=3$) than a plane. Fractal dimensions are also measures of the amount of space occupied, but they do not have integer values. The following example illustrates the difference between D and D_T. Any curve, such as those shown in Fig. 2, can be contained in a plane; thus $D_T=1$. However, the complex curves (Fig. 2b, c) have a much greater length than do simple curves (Fig. 2a); therefore, these convoluted and involuted curves have $D>1$. As curves becomes increasingly complex (i.e. plane-filling) in a self-similar fashion, D continues to increase, approaching an upper limit at the topological dimension of a plane (since no curve can take up more space than a plane). Thus, the fractal dimensions of all plan-view shapes of self-similar objects are in the range: $1<D<2$. The method by which fractal dimension is calculated is described below.

Bruno et al. (1992) showed that the flow margins of both endmember types of basaltic lavas (a'a and pahoehoe) are fractal, with the scale of self-similarity extending from about 0.5 m to over 2 km. This suggests that the processes that control the shapes of basaltic flows at a small (say, 1 m) scale are dynamically similar to the processes that control flow shapes at a 10 m or 100 m scale. For pahoehoe flows, this implies that the same factors that control the outbreak of a small toe control the outbreak of a larger eruptive unit. For a'a flows, which have crenulation-like features superimposed upon larger flow lobes, self-similarity implies that the same factors that cause these crenulations to form (presumably related to differential shear stress) are also responsible for forming the lobes themselves; i.e. the lobes are large-scale crenulations. Kilburn (1990) made a similar point in describing the fractal properties of the surfaces of a'a flows. Also, Bruno et al. (1992) discovered that the margins of a'a and pahoehoe flows have different fractal dimensions. Pahoehoe margins have higher D (typically ≥ 1.15) than do a'a flows (usually ≤ 1.09). This is consistent with our observation that outlines of pahoehoe margins are qualitatively different from a'a margins (Fig. 3); pahoehoe margins tend to have many more embayments and protrusions than the more 'linear' a'a margins.

These differences in geometry do not reflect differences in composition, but rather differences in rheology and emplacement mechanisms. Whether an erupting basalt becomes a'a or pahoehoe depends on a critical relationship between volumetric flow rate (largely controlled by effusion rate and ground slope), effective viscosity and shear strength (Shaw et al. 1968; Shaw 1969; Peterson and Tilling 1980; Kilburn 1981). Pahoehoe flows are associated with low terminal volumetric

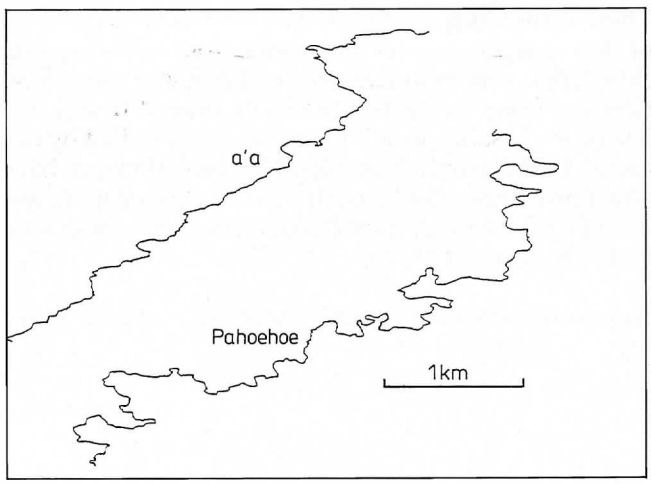

Fig. 3. Digitized outlines of typical a'a and pahoehoe flows from the 1935 eruption of Mauna Loa volcano. The pahoehoe margin is more convoluted than the a'a margin, and would be expected to have a higher D (following Bruno et al. 1992)

flow rates (typically $<10\ m^3/s$ for Hawaiian eruptions) and/or fluid lavas (Rowland and Walker 1990). They tend to be thin (<2 m) and advance with a smooth rolling motion (Cas and Wright 1987). Pahoehoe flows are formed in compound flow fields composed of numerous thin overlapping units. In contrast, a'a flows form at higher terminal flow rates. They are generally associated with higher effusion rates (typically $>10\ m^3/s$ for Hawaiian eruptions) and/or viscous lavas (Rowland and Walker 1990). A'a flows are generally thicker (typically a few meters), and have massive interiors and clinkery exteriors. Unlike most pahoehoe flows, they are erupted as a single unit. A'a and pahoehoe lavas also differ in mode of transport. Lava tubes can play crucial roles in transport of pahoehoe lavas, enabling flow over long distances with small radiative heat losses; a'a lavas typically flow in open channels. All of these differences in terminal flow rates, flow styles and emplacement mechanisms lead to different fractal dimensions for a'a and pahoehoe flows.

One of the objectives of investigations of flow morphology is to determine rheological properties and perhaps lava-flow composition, particularly SiO_2 and volatile content. So, in addition to basalts, we have studied more silicic flows with SiO_2 contents ranging from 52 to 74 wt %. Silicic flows can erupt as single-flow units characterized by a blocky morphology. They are also often associated with channel formation. Thus, in terms of both morphology and emplacement mechanism, some high-silica flows are similar to a'a flows and different from pahoehoe flows. We have found that higher silica contents and the accompanying increase in viscosity and presumable yield strength lead to qualitative as well as quantitative differences in plan-view shapes. Figure 4a shows a basaltic a'a flow, characterized by fairly linear margins, superimposed upon which are small-scale features that resemble crenulations. Figure 4b (basaltic andesite) has finger-like lobes, hundreds of meters in diameter, and appears less 'linear'. Like basaltic a'a, this basaltic andesite has a crenulated appearance. Figure 4c (andesite) also has multiple lobes. Here, the lobes appear shorter, stubbier and wider (approaching 1 km), and the crenulations appear to be absent. Figure 4d (dacite) is characterized by the highest silica content. Here the lobes are still wider (>1 km) and protrude less from the main mass of the lava flow, causing the flow to assume a more bulbous appearance. We note that silica content is just

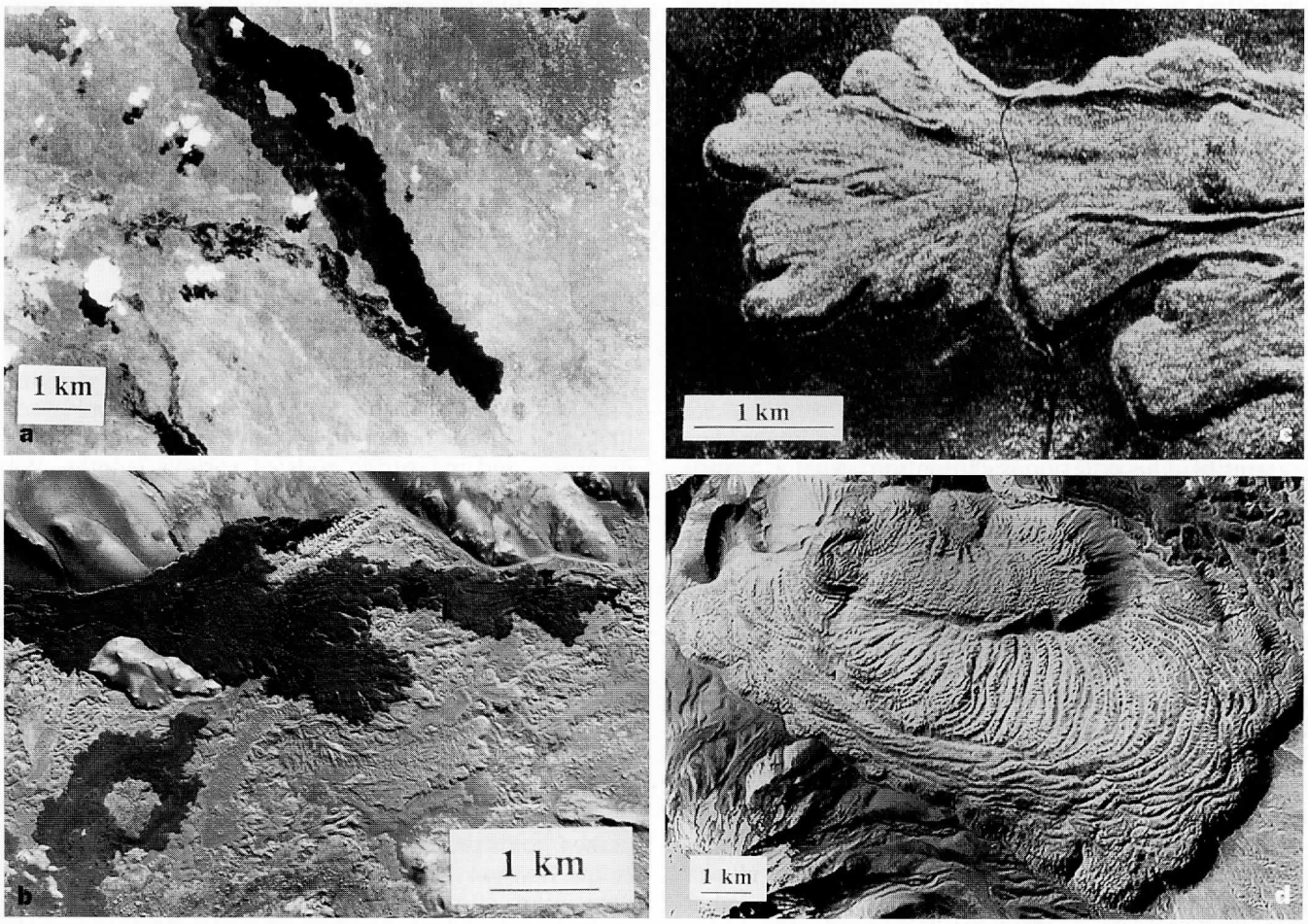

Fig. 4a–d. Plan-view shapes of lava flows of various compositions (in order of increasing silica content): **a** basalt (Galapagos Islands); **b** basaltic andesite (Hekla, Iceland); **c** andesite (Mount Shasta, US); **d** dacite (Chao, Chile). As silica content increases, flow lobes tend to widen, thicken and protrude less from the main mass of the lava flow, and the smaller-scale features become suppressed

one controlling factor on plan-view shape; there are many other controlling factors (e.g. overall volume, volatile content, eruption rate). Nevertheless each range of silica content (basalts, basaltic andesites, andesites, and dacites/rhyolites) appears to show qualitative differences in plan-view shape. In this paper, we quantify the effect of rheology on perimeters of lava flows using fractal analysis. Our objective is to define quantitative parameters that vary with rheology, which in combination, can be used to remotely distinguish flow types.

Methodology

The fractal analysis employed in this study uses three quantitative parameters: correlation coefficient (R^2), fractal dimension (D), and quadratic coefficient (a). These parameters are all calculated in accordance with the 'structured-walk' method (Richardson 1961). Alternative methods include 'equipaced polygon', 'hybrid walk' and 'cell-count' methods; these are discussed in detail in Longley and Batty (1989). We selected the structured-walk method because it can be readily applied, both in field measurements and from remote-sensing images. According to the structured-walk method, the apparent length of a lava-flow margin is measured by walking rods of different lengths along the margin. For each rod length (r), flow margin length (L) is determined according to the number of rod lengths (N) needed to approximate the margin; that is, $L = Nr$. By plotting log L vs log r (called a 'Richardson plot', after Richardson 1961), fractal behavior can be determined.

Calculating correlation coefficient (R)

A linear trend on a Richardson plot indicates the data form a fractal set, indicating self-similarity over the range of rod lengths used. Our criterion for linearity (i.e. fractal behavior) is an R^2 value exceeding 0.95, where R is the correlation coefficient of the linear least squares fit. This criterion is chosen somewhat arbitrarily, but follows that used by Mueller (1987). Care was taken to ensure that the data array did not artificially flatten out at long rod lengths as a result of choosing rod lengths that are so large such that they approach the length of the object. One can avoid this problem altogether by letting r approach the length of the object (that is, letting N approach 0) and plotting all the data on a Richardson plot. One can then visually select the linear portion of the curve and fit a least squares line to the selected segment. Although we have found this technique suitable in measurements of lava flows taken from aerial photographs, it is quite impractical in the field, as it would involve a large number of time-consuming measurements. We have found that choosing our longest rod length such that it can be placed at least five times along a flow margin (i.e. $N = 5$ is a minimum value) is sufficient to prevent this artifact from compromising our results.

Calculating fractal dimension (D)

The fractal dimension of a curve (such as a lava-flow margin) is a measure of the curve's convolution, or deviation from a straight line. The fractal dimension (D) can be calculated as:

$$D = 1 - m,$$

where m is the slope of the linear least squares fit to the data on the Richardson plot (see Turcotte 1991 for derivation and more detailed discussion). Because lava-flow margins are characterized by embayments and protrusions and smaller rods traverse more of these features, L increases as r decreases. Thus, the Richardson plot has a negative slope ($m < 0$) and $D > 1$.

Calculating quadratic coefficient (a)

In the above discussions of calculating fractal dimensions and correlation coefficients, the data on the Richardson plot are fit with a least squares line. Alternately, the data can be approximated by a second-order least squares fit and the quadratic coefficient (a) can provide insight into fractal tendency. An ideal fractal would be expected to have $a = 0$. (We tested this methodology on an ideal, computer-generated fractal and found $a = 0.002$). A negative value of a on a Richardson plot (concave-downward) translates to an increase in slope with increasing rod length, indicating a relative lack of small-scale features. A positive value of a (concave-upward) correlates with a decrease in slope with increasing rod length, or a relative lack of large-scale features.

Field measurement technique

We applied our methodology to lava-flow margins both in the field and on aerial photographs and other images. The field technique requires two people, a tape measure, and measuring rods of various lengths. We use wooden dowels to define the smaller rod lengths (1/8, 1/4, 1/2 and 1 m) and lightweight chains to define the longer rod lengths (2, 4, 8 and 16 m). First, we isolate a section of flow margin to be measured and, somewhat arbitrarily, choose a point along the margin as the starting point. When the selected section of flow margin is sufficiently long to permit, the measurement begins with one person holding one end of the 16 m chain at the starting point (a). A second person walks along the flow margin until the other end of the taut chain exactly intersects the outline. This new point (b) becomes the next starting point. Now, as the second person holds the end of the 16 m chain fixed over point b, the first person walks along the boundary until the next intersection point (c) is found. This process continues until a given number of lengths (N) are measured, and the ending point is marked. To maximize accuracy, the measurement is replicated using the same

Table 1. Directional analysis. N values obtained by replicating field measurement in opposite direction

r (meters)	N_1	N_2
16	5.00	5.02
8	11.52	10.81
4	26.73	25.55
2	63.61	63.63
1	140.10	140.19

chain length, but this time the persons walk in the opposite direction (from the ending point to the starting point). We have found that the N values from both directions match well (Table 1). The results (N) are averaged and L (in meters) is calculated as $L=Nr$. Ideally, this first length calculation (L_1) will be based on five lengths of a 16 m chain, so $L_1=80$ m.

We then recalculate the length of the same segment (L_2), using a chain half of the original length ($r=8$ m). Since the 8 m chain will, in all probability, record some undulations in the flow margin that were not encountered by the 16 m chain, $L_2>L_1$, implying $N_2>10$. Note that it is possible (and likely) that N_2 will be a fraction. We continue dividing the chain length by two and repeating the procedure until at least five measurements of L have been made using five different rod lengths, i.e. the Richardson plots have a minimum of five data points.

For sufficiently long flow-margin segments, these data points generally correspond to chain lengths of 1, 2, 4, 8, and 16 m. In some cases, we included an additional rod length of 0.5 m. For shorter flow-margin segments that cannot accommodate five lengths of a 16 m chain, the first (longest) chain length we chose is the longest chain length that can be walked along the flow margin at least five times. In these cases, rod lengths smaller than 1 m are necessarily used to meet the minimum requirement of five measuring rods/chains, separated by a factor of two in length. The smallest rod lengths used were 0.25 m for a'a flows and 0.125 m for pahoehoe flows.

Error and variation analyses of field measurement technique

We conducted analyses, based on field measurements, to confirm both the field measurement technique's precision ('error analysis') as well as its applicability to the entire flow margin ('variation analysis'). To assess the precision, we conducted five replicate measurements of a typical Hawaiian pahoehoe margin: a portion of the 1972 Mauna Ulu pahoehoe flow (Kilauea Volcano). We began each measurement at the same starting point, and measured off five lengths of a 16 m chain. Therefore, the ending points of each measurement did not necessarily coincide, but instead were chosen such that $L_1=80$ in each case. Each measurement consisted of five data points, corresponding to chain lengths of 1, 2, 4, 8 and 16 m. The results of this error analysis are summarized in Table 2. Note the negligible variance of D: $\sigma=0.008$. Although this error analysis implies that the technique is precise, it does not suggest that the calculated D of a given flow-margin segment is representative of the entire flow. Different segments of a flow margin may have different fractal dimensions, and this error analysis does not measure this segment-to-segment variation. Therefore, we performed an additional analysis on the 1972 Mauna Ulu pahoehoe flow to rigorously study variation along a flow margin. We measured D of seven adjacent segments of a flow margin in the field, with each segment defined as five lengths of a 16 m chain ($L_1=80$). These results, summarized in Table 3, show a significantly larger variation, with $\sigma=0.05$.

Table 2. Error analysis (field data of 1972 Mauna Ulu pahoehoe, segment 1)

Trial number	D	R^2
1	1.163	0.980
2	1.173	0.977
3	1.177	0.988
4	1.182	0.980
5	1.182	0.990
Mean D value:	1.175	
Standard deviation:	0.008	

Table 3. Variation analysis (field data of 1972 Mauna Ulu, pahoehoe)

Segment number	D	R^2
1 (avg.)	1.175	0.987
2	1.207	0.958
3	1.315	0.960
4	1.186	0.997
5	1.183	0.984
6	1.161	0.980
7	1.185	0.956
Mean D value:	1.202	
Standard deviation:	0.052	

Photographic measurement technique

A form of the same 'structured-walk method' was utilized to determine fractal dimensions of lava flows from aerial photographs and radar images, at scales ranging from 1:6000 to 1:70000. We tried to use flow margins in the centers of the images to avoid distortion.

The margins were digitized and the fractal dimensions calculated using the EXACT algorithm (Hayward et al. 1989). Computerization facilitates changing the rod lengths in small increments, improving the precision of the calculated D. We used 30 rod lengths, equally spaced on a log scale. (Using more than 30 rod lengths did not significantly improve the calculated D.)

Consistent with the field methodology, the minimum flow-margin segment included in the aerial photographic data set corresponds to N=5 for the longest rod length, and fractional N-values were permitted for subsequent rod lengths. The actual length of this longest rod depends on the scale of the image, and ranges up to 2.4 km. The minimum rod length was chosen to be sufficiently large as to exceed both the noise inherent in the digitization process as well as the spatial resolution of photographic images.

Error and variation analyses of photographic measurement technique

Analogous with our analyses of the field technique, we conduct error and variation analyses to confirm the photographic measurement technique. Since this technique is computerized, it is perfectly reproducible; every measurement taken from a given starting point will, after a certain amount of rod lengths are measured, result in the exact same ending point. Thus, any error analysis of fractal dimension would necessarily yield $\sigma=0$. In order to assess variation of fractal dimension among different segments of flow margin, we select the longest flow margin in the photographic database (Hell's Half Acre, pahoehoe). We divide this margin, which contains over 8000 data points, into seven overlapping flow-margin segments. Each of these segments contains 2000 points and overlaps adjacent segments by 1000 points. Thus segments 1, 3, 5, and 7 are non-overlapping, as are segments 2, 4 and 6. To be consistent with our field variation analysis, we would ideally like to have seven non-overlapping flow segments. However, data limitations prevent this. The results of this analysis, summarized in Table 4, show a comparable variation, with $\sigma=0.04$.

Data

The database consists of 55 lava flow margins (or segments thereof). The selected margin may be of an individual eruptive unit or a compound flow field. In choosing suitable candidates for measurement, we used the following 'simple-case' criteria: (1) The margin is continuous, well-preserved and unambiguous (e.g. not obscured by forest or younger flows); (2) It is unaffected by external controls, such as a steep ground slope or preexisting topography; (3) The segment is representative of the entire margin. We categorize the analyzed flows based on composition, separating the basalts from the more silicic flows. We further divide the more silicic flows based on silica content. This database is an extension of that considered by Bruno et al. (1992), which included 28 basaltic lava flows.

Table 4. Variation analysis (photographic data of Hell's Half Acre, pahoehoe)

Segment number	D	R^2
1	1.204	0.970
2	1.263	0.953
3	1.243	0.936
4	1.188	0.954
5	1.177	0.969
6	1.218	0.960
7	1.270	0.953
Mean D value:	1.223	
Standard deviation:	0.036	

Basaltic lava flows

This analysis of basaltic lava flows is based on two types of data: (1) field studies of 27 lava flows on Kilauea, Mauna Loa and Hualalai volcanoes on Hawaii. These flows have different morphologies, and include seven a'a, 16 pahoehoe and four 'transitional' flows, i.e. flows with morphologies intermediate between a'a and pahoehoe; (2) aerial photographs of 18 lava flows in Hawaii, the western US, Iceland, and the Galapagos Islands. These flows include eight pahoehoe and ten a'a. No transitional flows are included in the photographic database. Scales of photographs range from 1:6000 to 1:60000, which determine the rod lengths which range from 12 m to 2.4 km. Including the field data, the scale extends down to 0.125 m for pahoehoe flows and 0.25 m for a'a flows. The database for basaltic flows is summarized in Table 5a.

Silicic lava flows

This analysis of silicic lava flows is based exclusively on data obtained from aerial photographs and radar images; no field data have been taken to date. The database, summarized in Table 5b, consists of ten flows with silica contents ranging from 52 to 74%. We divide these flows into two categories based on silica content: basaltic andesites (SiO_2: 52–58%) and more silicic flows (SiO_2: 61–74%), the latter being primarily dacites and rhyolites. These images have scales ranging from 1:8250 to 1:70000, which determine the lengths of rods used (10 m–4.5 km).

Results and discussion: basaltic lava flows

Basaltic lava flow margins are fractals

Our preliminary results (Bruno et al. 1992) indicated that both a'a and pahoehoe flow margins are fractals within the range of scale studied (r: 0.5 m–2.4 km). Richardson plots are linear (Fig. 5), demonstrating self-similarity. The present analysis confirms that conclusion based on a larger database (45 flows) and over a wider range of scale (r: 0.125 m–2.4 km). Furthermore, transitional flows have also been shown to be fractal. The only cases where the margins of basaltic

Table 5a. Database of basaltic flows

Flow description	Flow type	D	R^2	Data type	Substrate (field data only)
Kilauea Volcano, Hawaii					
1971 Mauna Ulu	pahoehoe	1.19	0.962	field	ash
1972 Mauna Ulu	pahoehoe	1.20 (avg)	0.994	field	pahoehoe
1972 Mauna Ulu	pahoehoe	1.18	0.973	field	pahoehoe
1972 Mauna Ulu	pahoehoe	1.21	0.987	field	pahoehoe
1972 Mauna Ulu	pahoehoe	1.20	0.982	field	pahoehoe
1972 Mauna Ulu	a'a	1.05	0.990	field	pahoehoe
1972 Mauna Ulu	a'a	1.06	0.988	field	pahoehoe
1974 Mauna Ulu	pahoehoe	1.15	0.963	field	pahoehoe
1974 Mauna Ulu	transitional	1.10	0.975	field	pahoehoe
1974 Mauna Ulu	transitional	1.12	0.977	field	pahoehoe
1974 Mauna Ulu	a'a	1.07	0.987	field	pahoehoe
1974 Mauna Ulu	a'a	1.09	0.963	field	pahoehoe
1974 Mauna Ulu	a'a	1.08	0.965	field	pahoehoe
1977 Pu'u O'o	a'a	1.05	0.967	photo	
1982 Kilauea	pahoehoe	1.21	0.989	field	ash
1990 Pu'u O'o	pahoehoe	1.18	0.995	field	pahoehoe
Mauna Loa Volcano, Hawaii					
prehistoric, nr Saddle Rd	pahoehoe	1.23	0.988	field	a'a
prehistoric, nr Pu'u Ki	pahoehoe	1.23	0.997	field	a'a
prehistoric, nr Pu'u Ki	pahoehoe	1.12	0.954	field	pahoehoe
1843 Mauna Loa	a'a	1.11	0.972	photo	
1843 Mauna Loa	pahoehoe	1.15	0.969	field	pahoehoe
1852 Mauna Loa	pahoehoe	1.13	0.992	photo	
1855 Mauna Loa	pahoehoe	1.19	0.960	photo	
1855 Mauna Loa	pahoehoe	1.17	0.986	field	pahoehoe
1855 Mauna Loa	pahoehoe	1.19	0.979	field	a'a
1855 Mauna Loa	transitional	1.09	0.961	field	a'a
1859 Mauna Loa	a'a	1.07	0.965	photo	
1859 Mauna Loa	pahoehoe	1.14	0.970	field	a'a
1881 Mauna Loa	pahoehoe	1.17	0.970	photo	
1899 Mauna Loa	a'a	1.13	0.981	photo	
1935 Mauna Loa	a'a	1.08	0.973	photo	
1935 Mauna Loa	pahoehoe	1.20	0.956	photo	
1935 Mauna Loa	pahoehoe	1.15	0.988	field	a'a
1942 Mauna Loa	a'a	1.07	0.973	photo	
Hualalai Volcano, Hawaii					
1800 Hualalai	a'a	1.06	0.968	photo	pahoehoe
1800 Hualalai	transitional	1.15	0.992	field	pahoehoe
1800 Hualalai	a'a	1.09	0.967	field	pahoehoe
1800 Hualalai	a'a	1.08	0.995	field	pahoehoe
Non-Hawaiian Volcanoes					
Hell's Half Acre, Idaho	pahoehoe	1.21	0.981	photo	
Volcano Peak, California	pahoehoe	1.23	0.963	photo	
Fernandina, Galapagos	a'a	1.07	0.972	photo	
Fernandina, Galapagos	a'a	1.09	0.952	photo	
Fernandina, Galapagos	a'a	1.05	0.985	photo	
Krafla, Iceland	pahoehoe	1.16	0.971	photo	

flows are not fractal are on steep slopes. In these cases where the margin is externally controlled by a steep ground slope, the margin becomes more linear, with fewer convolutions.

The fractal behavior of pahoehoe and a'a flows might be predicted by their basaltic composition. Low viscosities of the order of 1000 Pa-s for typical eruption temperatures of 1150° C, coupled with a negligible yield strength for most basalts, offers no obstacle to prevent self-similar features from being formed on a wide range of scales. We note that at some small scale below the detection limit of this study, fractal behavior will eventually break down due to material properties.

Pahoehoe and a'a have different D

We find that over a wide range of geographic locations (Hawaii, Iceland, western US, Galapagos Islands), basaltic lavas divide into two populations with regard to their fractal dimensions. A'a flows generally have D

Table 5b. Database of silicic flows

	Flow description	SiO_2 (%)	Flow type	Scale of image	Reference
1	Andes Mountains	52	Bas. Andesite	1:27000	Thorpe et al. (1984)
2	Andes Mountains	52	Bas. Andesite	1:13500	P Francis (personal communication)
3	1980 Hekla, Iceland	55	Bas. Andesite	1:8250	Gudmundsson et al. (1991)
4	1991 Hekla, Iceland	55	Bas. Andesite	1:21500	Gudmundsson et al. (1991)
5	SP Flow, Arizona	57	Bas. Andesite	1:36000	Ulrich and Bailey (1987)
6	Lava Park Flow, California	61	Andesite	1:30000	Smith and Carmichael (1968)
7	Ludent, Iceland	65	Dacite	1:8250	Nicholson (personal communication)
8	1104 Hekla, Iceland	65	Dacite	1:8250	Sigmarsson (personal communication)
9	Chao, Chile	66	Dacite	1:70000	Guest and Sanchez (1969)
10	Glass Mountain, California	74	Rhyolite	1:12000	Eichelberger (1975)

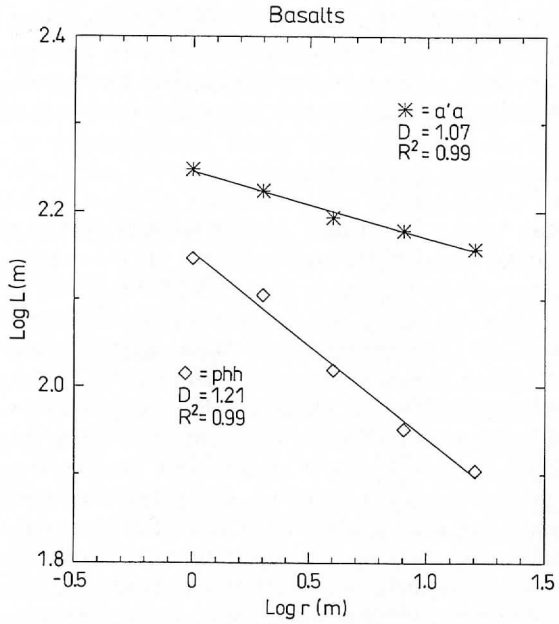

Fig. 5. Richardson plots of typical a'a and pahoehoe flows, in meters, based on field data. High R^2 values (>0.95) indicate fractal behavior. The more convoluted margins of pahoehoe flows translate to higher D

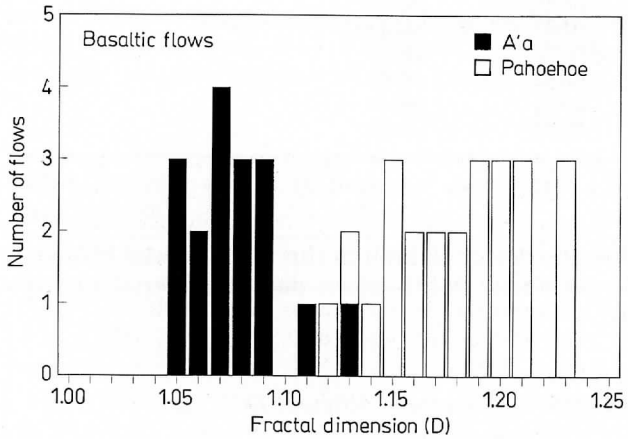

Fig. 6. Histogram of D values of a'a and pahoehoe flows based on field and photographic data. Both field and photographic measurements show pahoehoe flows have higher D than a'a flows. Transitional flows (not shown) tend to have intermediate D

ranging between 1.05 and 1.09 whereas pahoehoe flows typically have D ranging between 1.15 and 1.23. Figure 6 summarizes our results for basaltic flows. Most (12 of 14) of the Hawaiian a'a flows have D between 1.05 and 1.09; all have D between 1.05 and 1.13. Most Hawaiian pahoehoe flows (18 of 21) have D between 1.15 and 1.23; all have D between 1.12 and 1.23. The two pahoehoe flows in the western US yield measurements of 1.21 and 1.22, consistent with the range of Hawaiian pahoehoe flows. Similarly, the Krafla, Iceland basalt (pahoehoe) falls into the Hawaiian pahoehoe range, with a fractal dimension of 1.16. The three Galapagos flows measured, all a'a, yield D values of 1.05, 1.07 and 1.09, in agreement with the range of Hawaiian a'a flows. This is good evidence that regardless of the exact nature of the eruption, the pahoehoe flows consistently have higher D than a'a flows.

By definition, fractals should have constant ranges of fractal dimensions, regardless of the rod lengths used to measure D. Thus, if lava flows are fractals over the range of scale studied, the fractal dimensions obtained at the field scale (0.125–16 m) should be similar to the range of fractal dimensions obtained at the aerial photographic scale (12 m–2.4 km) for a'a as well as pahoehoe. This is confirmed by our results. All seven a'a flows measured in the field have D between 1.05 and 1.09 (Fig. 6), the same range we find for photographic data of a'a flows (Fig. 6). All 16 pahoehoe field measurements have D between 1.12 and 1.23, compared with a range of 1.13–1.23 for photographic data of pahoehoe flows.

For three flows (all pahoehoe), we measured margins of the same flow in the field and from aerial photographs. The fractal dimensions as measured from aerial photographs are 1.19 (1855 Mauna Loa), 1.14 (1859 Mauna Loa) and 1.20 (1935 Mauna Loa). Field measurements yielded corresponding D of 1.17, 1.16 and 1.15, respectively. These variations in D are within the variation of Table 3, and indicate fractal behavior.

Flows that we have determined to be transitional between a'a and pahoehoe based on field observations tend to have intermediate fractal dimensions, as might be expected. Of the four field measurements of transitional flows, three have D between 1.09 and 1.12; the fourth has a slightly higher D of 1.15.

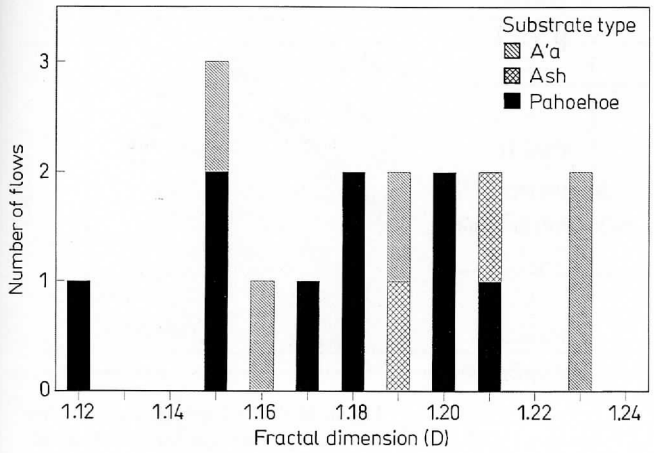

Fig. 7. Histogram of D values of pahoehoe flows on three different substrates – preexisting a'a or pahoehoe flow, or ash – based on field data. There is no apparent correlation between D and substrate type

One might expect that the fractal dimensions of flow margins would be affected by the nature of the substrate over which they flowed. A pahoehoe margin might be different on a preexisting a'a flow compared to a preexisting pahoehoe flow. However, a detailed analysis shows that D values are unaffected by differences in substrate. We took 16 field measurements of Hawaiian pahoehoe flows. Some of these lavas flowed upon preexisting a'a lava flows (5), others upon preexisting pahoehoe flows (9), still others atop ash deposits (2). Figure 7 shows the lack of correlation between D and substrate for these 16 flows. In one case (1855 Mauna Loa pahoehoe), we performed a controlled experiment on the effect of substrate on D. We measured D in one location where this pahoehoe flowed over a preexisting pahoehoe, and again nearby (within 100 m), where the same flow covered an a'a substrate. The D values obtained for this flow overlying pahoehoe and a'a substrates (1.17 and 1.19, respectively) are well within the observed variation of D along a flow margin with a constant substrate (see Table 3).

Clearly, a pattern emerges for the fractal dimensions of terrestrial basaltic lava flows. Regardless of geographic location, lengths of rods used, or substrate material, pahoehoe flow margins consistently have higher D than a'a flow margins within the range of scale studied. This is consistent both with the preliminary results of Bruno et al. (1992) and also the observation that the outlines of pahoehoe and a'a flows are qualitatively different.

A note about topographically controlled flows

Topographically controlled flows have been excluded from this analysis because these external controls can have a significant effect on D. Positive topography (e.g. hills) may deflect or bifurcate flows, increasing the degree of flow-margin convolution and therefore increasing D. Negative topography (e.g. channels) serves to confine or channelize flows, causing the margin to become more linear and thus decreasing D. In many cases, these external controls interfere with the development of self-similar features, and prevent fractal behavior. Similarly, we have found fractal behavior to break down, with an accompanying decrease in D, on steep (>15–28°) slopes (see Table 6). This tendency toward nonfractal behavior as the gravity-driven force on the flow increases is consistent with the results presented in Baloga et al. (1992).

Table 6. Slope analysis. Effect of slope on fractal properties of 1972 Mauna Ulu a'a flow (field data)

Flow Description	Flow type	D	R^2	Slope
1972 Mauna Ulu	a'a	1.046	0.990	11.6°
1972 Mauna Ulu	a'a	1.055	0.988	14.7°
1972 Mauna Ulu	a'a	1.023	0.778	27.8°

Implications for flow dynamics

The fractal properties of lava flows may offer insight into the dynamics of flow emplacement because fractals reflect nonlinear processes (e.g. Campbell 1987). We have made a preliminary evaluation of the nonlinear aspects of flow dynamics to obtain a qualitative indication of the tendency toward fractal behavior. Following earlier fluid dynamic models (e.g. Baloga and Pieri 1986; Baloga 1987), we depict variations in the free surface of a lava flow as due to a balance between a gravitational transport term and the fluid dynamic ('magmastatic') pressure gradient. Baloga et al. (1992) define two dimensionless parameters (p and q) to describe the relative importance of these two influences. The parameter p is the ratio of the pressure gradient to gravitational terms; the parameter q is an absolute measure of the gravitational force on the flow. Baloga et al. (1992) developed a governing equation for the three-dimensional surface of a lava flow during emplacement, based on simplifying assumptions:

$$\partial h/\partial t + q\,h^2(\partial h/\partial x) = p\,q\,\partial/\partial y\,[h^3(\partial h/\partial y)]$$

where

$$p = \cot\theta\, h_0 L/(3w^2)$$

$$q = g\sin\theta\, h_0^2 T/(\nu L)$$

and where x and y are the downstream and cross-stream directions respectively, h = flow thickness, t = time; h_0, L, w and T are scales for thickness, length, width and time, respectively; θ = slope, ν = kinematic viscosity and g = gravitational acceleration.

By assuming $\partial h/\partial t$ is on the order of 1, Baloga et al. (1992) evaluated this equation for selected values of p and q (Fig. 8). High p values (right column of the matrix) indicate the magmastatic pressure gradient is important relative to gravity. Low q values (top row of matrix) indicate a weak gravitational term. Thus, in case 1c (large p, small q), the gravitational term is the least important, both relatively (to the pressure gradient) and absolutely, and the magmastatic pressure

	$p \ll 1$	$p = 1$	$p \gg 1$
$q \ll 1$	**Case 1a** $\partial h/\partial t = 0$	**Case 1b** $\partial h/\partial t = 0$	**Case 1c** Assume $pq = 0(1)$ $\partial h/\partial t = \partial/\partial y[h^3(\partial h/\partial y)]$
$q = 1$	**Case 2a** $\partial h/\partial t + h^2(\partial h/\partial x) = 0$	**Case 2b** $\partial h/\partial t + h^2(\partial h/\partial x) = \partial/\partial y[h^3(\partial h/\partial y)]$	**Case 2c** $0 = \partial/\partial y[h^3(\partial h/\partial y)]$
$q \gg 1$	**Case 3a** Assume $pq = 0(1)$ $h^2(\partial h/\partial x) = 0$	**Case 3b** $h^2(\partial h/\partial x) = \partial/\partial y[h^3(\partial h/\partial y)]$	**Case 3c** $0 = \partial/\partial y[h^3(\partial h/\partial y)]$

Fig. 8. Matrix of special cases of the governing equation for selected values of p and q, obtained by assuming $\partial h/\partial t$ is on the order of 1. Some of the equations in the matrix are linear; others are nonlinear. The linear equations would not be expected to produce fractals, whereas the nonlinear equations could be expected to produce fractals. See text for details

gradient dominates. Thus, since the lava flow is being largely driven by internal fluid dynamic forces in case 1c, we predict that this combination of p and q is likely to produce fractal behavior. As expected, the resulting diffusion equation is explicitly nonlinear.

For the same q ($q \ll 1$), consider the cases corresponding to p values that are low (case 1a) and moderate (case 1b). Both of these equations are linear, and would therefore not be expected to produce fractals. Since p is proportional to the ratio of magmastatic pressure gradient to gravitational driving force, this has important implications for the effect of gravity on fractal behavior. When gravity plays a non-negligible role (small or moderate p), the matrix predicts that the lava-flow margin would not be fractal. This is consistent with our field observations on Hawaii that flow outlines are not fractals when slopes are steep.

Case 2b is nonlinear diffusion with a kinematic transport term. Case 3b is the steady-state nonlinear diffusion equation. These are also likely candidates for producing fractals. Cases 2c and 3c are both nonlinear and are dominated by the pressure gradient term ($p \gg 1$). These cases may be expected to produce fractal behavior, but are difficult to interpret physically.

This analysis suggests that nonlinear processes are common in lava flows, particularly in those cases where the magmastatic pressure gradient influence is significant relative to the influence of gravitational transport. These nonlinear equations are candidates for producing fractals, provided they are physically plausible. Further studies are underway to (1) test this physical plausibility by continued comparison of theoretical prediction and field measurements and (2) extend the underlying physics to include more complex rheologic properties for lava flows of different compositions.

Results and discussion: silicic lava flows

Silicic lava flows are generally not fractals

Silicic lava flows are generally not fractals within the range of scale studied (r: 10 m–4.5 km). Typical Richardson plots for basalt, basaltic andesite, and dacite are shown in Fig. 9. Unlike the basaltic case, the Richardson plots for basaltic andesite and dacite are nonlinear, characterized by relatively low R^2 values. Instead of fractal behavior, these Richardson plots exhibit scale-dependent behavior: longer rod lengths have steeper slopes, most notably for the dacite. Thus, D tends to increase as r increases, contradicting the definition of D as a scale-independent parameter. This breakdown of fractal behavior at increased silica content is presumably related to the higher viscosities and yield strengths, which suppress smaller-scale features and thus prevent self-similarity over a wide range of scales.

Quantifying the effect of silica content on D

We seek to develop parameters that can be used remotely to quantify the effect of increasing silica content on fractal properties by comparing basalts, basaltic andesites, and dacites/rhyolites for two main purposes: (1) to gain insights into yield strength and rheological processes, and (2) to develop a remote-sensing tool that can differentiate flow type based on plan-view shape. Our approach is to use the study of basaltic flows as a benchmark for comparison with the more silicic flows. However, we restrict our basaltic 'benchmark' to a'a flows, which are similar to silicic flows in terms of both morphology and emplacement mechanism.

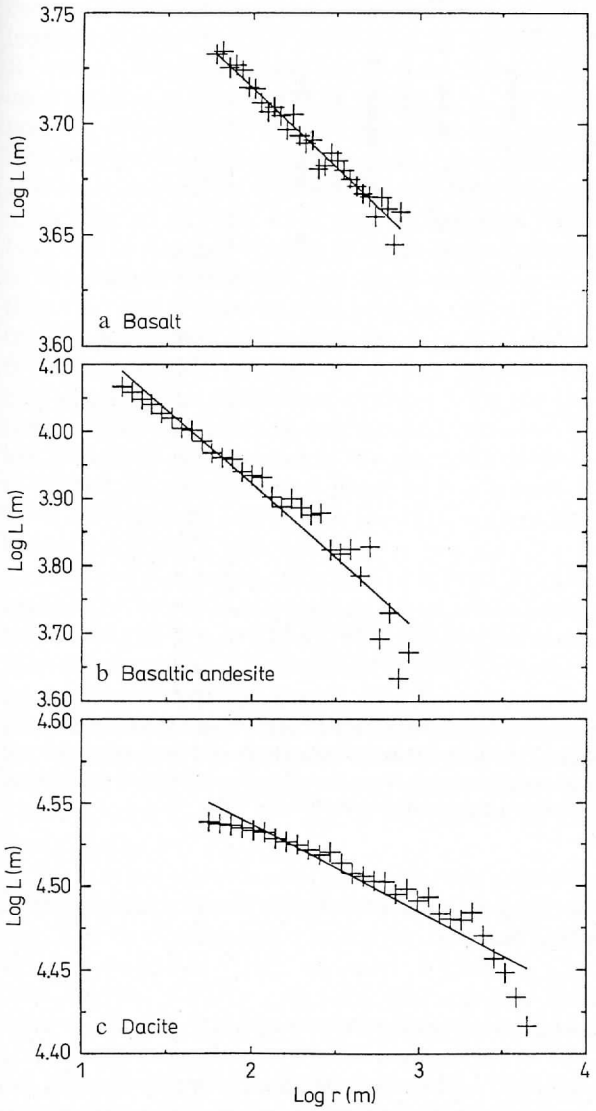

Fig. 9a–c. Richardson plots of representative **a** a'a basalt (Galapagos Islands); **b** basaltic andesite (Hekla, Iceland); **c** dacite (Chao, Chile), based on image data. Note that the data in (a) are closely approximated by a straight line, whereas the data for the higher silica flows (b, c) are not linear

Ideally, we would like to compare D of silicic flows to basaltic flows, to see how D changes with silica content. However, this approach is tricky because, as noted above, silicic flows are generally not fractals; instead D tends to increase with r for the majority of the silicic flows. Hence, the concept of a scale-independent fractal dimension for silicic flows is not valid. However, small regions of log r can be locally fit with a line. Here we introduce the concept of a 'local fractal dimension'. This does not imply the data set is fractal, nor that the local fractal dimension is scale-independent. It simply exploits our observation that select regions of the data can be fit by a line and we can estimate locally the degree of convolution for a selected range of rod lengths. Here we describe two methods used to compare silicic and basaltic flows. Both of these methods are sensitive to – and based on – our observation that silicic flows do not have scale-independent fractal dimensions.

Method 1: disjoint subsets of log r

This method dissects the abscissa of the Richardson plot into disjoint subsets of log r. The specific choice of subsets (summarized in Table 7a) is constrained by the data. Each of these subsets is fit locally by a least squares line; that is, the Richardson plot is fit by a series of lines. For each line, the slope (m) is calculated, and local fractal dimension D is calculated as 1 – m, consistent with our methodology for basaltic flows. Since this method can be used to describe fractals as well as non-fractals, it can be employed to compare basaltic and silicic lava flows.

Figure 10 shows sample Richardson plots of basalt, basaltic andesite and dacite, with the abscissa dissected according to the methodology described above. The data on these plots are the same as shown in Fig. 9; the only difference is the number of lines used to fit the data. Note that for the basalt, the three segments have essentially the same slope. This is consistent with our conclusion that basalts are fractals. Unlike the basalts, the basaltic andesite and dacite show noticeable differences in slope among the various subsets.

By plotting D of these segments vs. log r for the entire database of silicic flows, patterns begin to emerge among the basaltic andesites and the more silicic flows (primarily dacites and rhyolites). The basaltic andesites have roughly the same D values for the first two subsets (Fig. 11). At rod lengths of about 100 m ($\log r = 2$ m), D starts to increase, and the values also have a greater scatter. For the first three subsets of log r, the dacites/rhyolites have D plotting in a rather compact area, showing only negligible differences among the various ranges. At $\log r \sim 2.5$ m, D apparently begins to increase. We can use this technique to distinguish basaltic andesites from the more silicic flows. Both have a general increase in D with longer r, but the basaltic andesites tend to have greater D for each of these categories. Furthermore, the fact that dacites/rhyolites show negligible changes within the first three subsets ($\log r < 2.5$ m), whereas the basaltic andesites only remain relatively constant for the first two

Table 7. Ranges of log *r* (meters) for **a** Method 1 and **b** Method 2

a	METHOD 1	
		Log r (meters)
	Range 1:	<1.5
	Range 2:	1.5–2.0
	Range 3:	2.0–2.5
	Range 4:	2.5–3.3
b	METHOD 2	
		Log r (meters)
	Range 1:	1.7–2.8
	Range 2:	1.7–2.5
	Range 3:	1.3–2.0

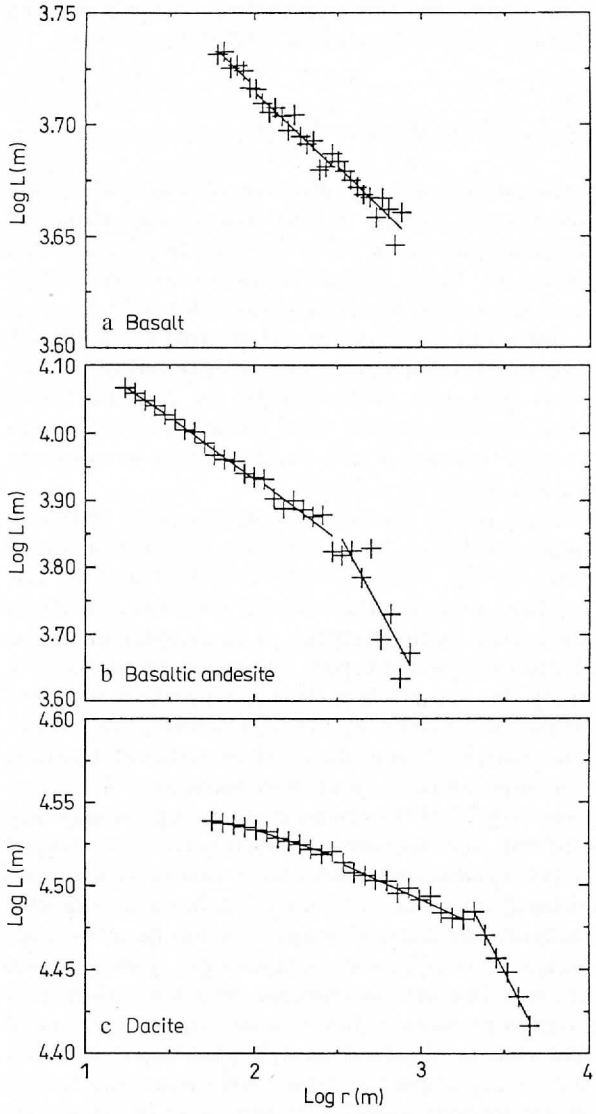

Fig. 10. Dissected Richardson plots of representative samples of **a** a'a basalt (Galapagos Islands); **b** basaltic andesite (Hekla, Iceland); **c** dacite (Chao, Chile), based on photographic data (same data as Fig. 9). Here, the abscissa is dissected into ranges of log r (Table 7a), and each range is locally fit with a straight line. Local fractal dimension is calculated as $D = 1 - m$, where m is the local slope as calculated according to Method 1. From left to right of these Richardson plots (increasing r), these local fractal dimensions are: **a** $D = 1.07$ for each segment; **b** $D = 1.17, 1.19, 1.19, 1.46$. (c) 1.02, 1.03, 1.05, 1.20. Note that D values are constant for (a), but not for (b) and (c). See text regarding Method 1

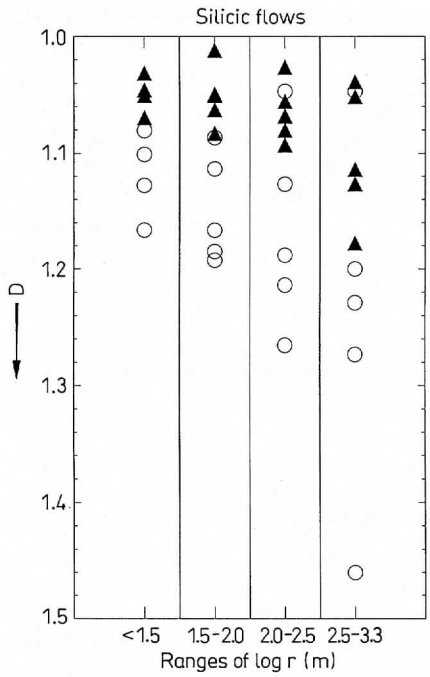

Fig. 11. Summary of 'local fractal dimension' (D) based on photographic data for entire database of silicic flows. Basaltic andesites are shown as *open circles,* whereas dacites and rhyolites are shown as *solid triangles.* Note that D is not a constant function of log r indicating non-fractal behavior

subsets ($\log r < 2.0$ m), is apparent. Figure 11 also emphasizes that D is not a constant function of log r for both basaltic andesites and dacites/rhyolites, indicating scale-dependent (non-fractal) behavior. Fractals such as basalts have relatively constant fractal dimensions across the various subsets. However, a sufficiently large range of log r is needed to discern fractal and non-fractal behavior. Note that a'a basalts and dacites have a similar range of fractal dimensions for the first three categories. Since data limitations often prevent obtaining such a large range of log r, we invoke a second method to differentiate a'a basalts from dacites, described below.

Method 2: overlapping subsets of log r

Like Method 1, this method dissects the abscissa of the Richardson plot into distinct regions of log r. However, it is different from the previous method in two respects. First, the selected ranges (as summarized in Table 7b) of log r are overlapping. Although the exact choice of ranges is again constrained by the data, they were intentionally chosen to overlap. This is to explicitly show the effect of a restricted range of rod lengths on local fractal dimension. For example, by comparing Region 1 (log r: 1.7–2.8 m) and Region 2 (log r: 1.7–2.5 m), we can explicitly see the effect of a restricted range of log r (2.5–2.8 m) on D and R^2. Second, as these regions span a greater range of log r than those in Method 1, we have sufficient data points to fit a second-order least squares curve to the data, in addition to the standard first-order least squares line. In this method, we fit a curve of the form $y = ax^2 + bx + c$, and note the value of the leading (or quadratic) coefficient *a*. In summary, this method compares three quantitative parameters (D, R^2, *a*) for three overlapping ranges of log r.

Applying Method 2 to dacites and rhyolites, we note systematic variation in D, R^2 and *a* with range of rod length. In four out of five cases, the longest rod lengths (Range 1) have the highest D and the lowest

corresponding R^2 values, whereas the shortest rod lengths (Range 3) have the lowest D and the highest R^2 values. Fitting a quadratic curve to Range 1 in each case yields a negative *a*. For Range 3, *a* can be either positive or negative. The D, R^2 and *a* for the dacites/rhyolites provide remarkably consistent results: all suggest scale-dependent (or non-fractal) behavior, characterized by an increase in D with increasing r. We attribute this to the suppression of small-scale features, due to the higher viscosities and yield strengths of silicic flow. We suggest the margin appears 'linear' to a certain range of small rod lengths because the scale of features they would otherwise detect are suppressed. This explains a fractal dimension close to 1 for the shortest range of rod lengths and, as expected, the corresponding R^2 values are quite high. We interpret these results to suggest that the shortest range of rod lengths (log r: 1.3–2.0 m) detects features in the flow margin that are below the limit of self-similarity.

We now present the results of Method 2 applied to basalts (i.e. those basalts which we measured using the ranges of r shown in Table 7b). Fractal dimension and the corresponding R^2 values show no systematic variation with range of rod length. The R^2 values are high, generally exceeding 0.95. The parameter *a* can be positive or negative, is generally close to zero, and again shows no systematic pattern among the various ranges. These results for D, R^2 and *a* for basalts all suggest fractal behavior.

We can use these fractal parameters to remotely differentiate flow types. Basaltic a'a and basaltic andesites can be distinguished primarily by their D values; basaltic andesites generally have higher D (≥ 1.15) than basaltic a'a (D: 1.05–1.09) and are less likely to exhibit fractal behavior. Although dacites/rhyolites and basalts have similar fractal dimensions (1.05–1.10) for extensive ranges of log r, dacites and rhyolites distinctly show non-fractal behavior. Systematic evaluation of D, R^2, and *a* at different range of rod lengths (as done in Method 2) can be used to distinguish dacites and rhyolites from basalts remotely.

There may be a critical value of r, related to silica content, which serves as a boundary for self-similar behavior (i.e. a value of r above which the flow appears fractal). This critical value may be related to lobe dimensions and/or the degree of suppression of smaller-scale features. Note that Fig. 11 shows a marked increase in D for dacites after about log r of 2.5 m ($r = 300$ m). This may be related to the lobe width of dacites, typically hundreds of meters. If so, we would expect the apparent D of basaltic andesites to increase at shorter rod lengths. This may be suggested by Fig. 11 but our database is too small to be conclusive. We believe that a larger database of silicic flows would reveal a critical value of breakdown of fractal behavior related to silica content. The fact that basaltic andesites appear to have relatively constant fractal dimensions up to $\log r = 2$ m while dacites/rhyolites appear to have relatively constant fractal dimensions up to $\log r = 2.5$ m suggests an effect of yield strength which is related to silica content. Our field observations shows that fractal behavior for basalts also breaks down, but at $r < 10$ cm.

The suppression of smaller-scale features in silicic flows implies that nonlinear instabilities are also suppressed inside the flows. Either the sluggish rheology prevents their formation, or it prevents their growth by rapidly damping out feedback mechanisms. The generally non-fractal nature of the margins of silicic flows is consistent with our simplified flow model (Fig. 8). Viscosities of silicic flows are very large, $>10^6$ for basaltic andesites and $>10^8$ for dacites and rhyolites, so q is certainly $\ll 1$. Thus, unless the flows have very large initial pressures, it is likely that their behavior would tend to be linear.

Conclusions

1. Basaltic lava flows are fractals

Bruno et al. (1992) suggested that basaltic lava flows are fractals, with pahoehoe flow margins having higher fractal dimension (1.13–1.23) than a'a flow margins (1.05–1.09). This study, based on a larger database (45 flows) and over a wider range of scale (0.125 m–2.4 km), confirms that earlier conclusion. Richardson plots are consistently linear, characterized by high R^2 values. Furthermore, we have shown that basaltic lava flows having transitional morphologies also exhibit fractal behavior, and tend to have dimensions intermediate between a'a and pahoehoe. This indicates that basaltic lavas, regardless of the emplacement mechanism, exhibit self-similar behavior. We interpret this to suggest that basalts are sufficiently fluid and lack a sizeable yield strength, offering no obstacle to deter the formation of small-scale self-similar features.

2. Silicic flows are generally not fractals

Unlike basalts, silicic lava flows tend to exhibit scale-dependent (non-fractal) behavior within the range of scale studied (r: 10 m–4.5 km). Typical Richardson plots for basaltic andesites and (especially) the more silicic dacites and rhyolites are non-linear. This breakdown of fractal behavior at increased silica content is presumably related to the higher viscosities and yield strengths, which suppress smaller-scale features.

3. Flow dynamics are nonlinear

Our observations that basaltic lava flows have fractal outlines when they are internally controlled yet have non-fractal outlines when they are controlled by gravitational forces are consistent with our theoretical model. An assessment of flow dynamics suggests that nonlinear processes operate for lava-flow emplacement on relatively flat slopes. These nonlinear mechanisms are damped out in silicic flows, leading to non-fractal margins, especially at small rod lengths.

4. *Quantifying the effect of rheology*

One of the primary objectives of this study is to remotely distinguish flow types. We suggest that fractal dimension (or local fractal dimension), correlation coefficient, and quadratic coefficient can be used, in combination, to attain this objective. We define 'local fractal dimensions' for select ranges of log r, and find that D tends to increase with increasing r after certain critical rod lengths are exceeded. We can use local fractal dimension to differentiate basaltic andesites from dacites and rhyolites. Although basaltic a'a and dacites have similar fractal dimensions over a wide range of r, the parameters R^2 and a can be used to remotely differentiate between these flow types.

Acknowledgements. This research was funded by the following National Aeronautics and Space Administration (NASA) grants: NGT 50930 (NASA Graduate Student Researchers Program), NAGW 3684 and NAGW 1162 (NASA Planetary Geology and Geophysics Program). Additional support was provided by the University of Hawaii Project Development Fund and Harold T Stearns Foundation. This manuscript benefited from reviews by H Shaw and G Valentine. Images were kindly provided by Duncan Munro (Galapagos Islands mosaic), Rosaly Lopes-Gautier and Peter Mouginis-Mark (Western US), Peter Francis (Andes) and Thorvaldur Thordarson (Iceland). Paul Lucey and Harold Garbeil provided software support. Many thanks go to Michelle Tatsumura for field assistance. This is IGP Publication No. 764 and SOEST Contribution No. 3578. This work forms part of the PhD dissertation of B Bruno.

References

Baloga S (1987) Lava flows as kinematic waves. J Geophys Res 92:9271–9279

Baloga S, Pieri D (1986) Time-dependent profiles of lava flows. J Geophys Res 91:9543–9552

Baloga S, Taylor GJ, Bruno BC (1992) The character of lava flow margins. Lunar Planet Sci XXIII:57–58

Bruno BC, Taylor GJ, Rowland SK, Lucey PG, Self S (1992) Lava flows are fractals. Geophys Res Lett 19:305–308

Campbell DK (1987) Nonlinear science. Los Alamos Science 15:218–262

Cas RAF, Wright JV (1987) Volcanic successions. Allen & Unwin, London, 528 pp

Crisp J, Baloga S (1990) A method for estimating eruption rates of planetary lava flows. Icarus 85:512–515

Eichelberger JC (1975) Origin of andesite and dacite: Evidence of mixing at Glass Mountain in California and at other circum-Pacific volcanoes. Geol Sci Am Bull 86:1381–1391

Fink JH (1980) Surface folding and viscosity of rhyolite flows. Geology 8:250–254

Fink JH, Fletcher RC (1978) Ropy pahoehoe: Surface folding of a viscous fluid. J Volcanol Geotherm Res 4:151–170

Garcia L (1991) The fractal explorer. Dynamic Press, Santa Cruz, 108 pp

Gudmundsson A, Oskarsson N, Gronvold K, Saemundsson K, Sigurdsson O, Stefansson R, Gislason SR, Einarsson P, Brandsdottir B, Larsen G, Johannesson H, Thordarson Th (1991) The 1991 eruption of Hekla, Iceland. Bull Volcanol 54:238–246

Guest JE, Sanchez J (1969) A large dacitic lava flow in northern Chile. Bull Volcanol 33:778–790

Hayward J, Orford JD, Whalley WB (1989) Three implementations of fractal analysis of particle outlines. Comp & Geosci 15:199–207

Hulme G (1974) The interpretation of lava flow morphology. Geophys J R Astron Soc 39:361–383

Hulme G, Fielder G (1977) Effusion rates and rheology of lunar lavas. Philos Trans R Soc London A285:227–234

Kilburn CRJ (1981) Pahoehoe and aa lavas: A discussion and continuation of the model of Peterson and Tilling. J Volcanol Geotherm Res 11:373–382

Kilburn CRJ (1990) Surfaces of aa flow fields on Mount Etna, Sicily: Morphology, rheology, crystallization, and scaling phenomena. In: Lava flows and domes (Fink JH, ed), Springer Verlag, Berlin: 129–156

Longley PA, Batty M (1989) Fractal measurement and line generalization. Comp & Geosci 15:167–183

Lopes RMC, Kilburn CRJ (1990) Emplacement of lava flow fields: Applications of terrestrial studies to Alba Patera, Mars. J Geophys Res 95:14383–14397

Mandelbrot BB (1967) How long is the coast of Britain? Statistical self-similarity and fractional dimension. Science 156:636–638

Mandelbrot BB (1983) The fractal geometry of nature. Freeman, San Francisco, 468 pp

Mueller J-C (1987) Fractal and automated line generalization. Cartographic J 24:27–34

Peterson DW, Tilling RI (1980) Transition of basaltic lava from pahoehoe to aa, Kilauea volcano, Hawaii: field observations and key factors. J Volcanol Geotherm Res 7:271–293

Richardson LF (1961) The problem of contiguity: an appendix to statistics of deadly quarrels. General Systems Yearbook 6:139–187

Rowland SK, Walker GPL (1990) Pahoehoe and aa in Hawaii: volumetric flow rate controls the lava structure. Bull Volcanol 52:615–628

Shaw HR (1969) Rheology of basalt in the melting range. J Petrology 10:510–535

Shaw HR, Swanson DA (1970) Eruption and flow rates of flood basalts. In: Proceedings of the Second Columbia River Basalt Symposium (Gilmour EH, Stradling D, eds), Eastern Washington State College Press, Cheney, 271–299

Shaw HR, Wright TL, Peck DL, Okamura R (1968) The viscosity of basaltic magma: An analysis of field measurements in Makaopuhi lava lake. Am J Sci 266:225–264

Smith AL, Carmichael ISE (1968) Quaternary lavas from the Southern Cascades, Western USA. Contrib Min Petrol 19:212–238

Thorpe RS, Francis PW, O'Callaghan L (1984) Relative roles of source composition, fractional crystallization and crustal contamination in the petrogenesis of Andean volcanic rocks. Philos Trans R Soc London A310:675–692

Turcotte DL (1991) Fractals in geology: What are they and what are they good for? Geol Sci Am Today 1, 1:3–4

Ulrich GE, Bailey NG (1987) Geologic Map of SP Mountain part of San Francisco Volcanic Field, North-Central Arizona. USGS Misc Field Map MF–1956

Wadge G, Lopes RMC (1991) The lobes of lava flows on Earth and Olympus Mons, Mars. Bull Volcanol 54:10–24

Walker GPL (1973) Lengths of lava flows. Philos Trans R Soc London A274:107–118

Editorial responsibility: D. Dzurisin